ELSEVIER

Journal of Molecular Catalysis A: Chemical 111 (1996) 145–165

JOURNAL OF MOLECULAR CATALYSIS A: CHEMICAL

Characterization and performance of a $[PtMo_6]/MgO$ catalyst for alkane-to-alkene conversion

D.I. Kondarides [1], K. Tomishige, Y. Nagasawa, U. Lee [2], Y. Iwasawa *

Department of Chemistry, Graduate School of Science, The University of Tokyo, Hongo, Bunkyo-ku, Tokyo 113, Japan

Received 31 January 1996; accepted 11 March 1996

Abstract

A novel $[PtMo_6]/MgO$ ensemble catalyst was prepared by using an inorganic cluster $[PtMo_6O_{24}]^{8-}$ as precursor and characterized by X-ray absorption fine structure (XAFS) spectroscopy. The EXAFS analysis revealed that platinum and molybdenum atoms interact with MgO support after calcination at temperatures above 673 K, making Pt–O, Pt–Mg and Pt–O (long) bonds, and Mo–O and Mo–Mg bonds, respectively. It was suggested that Pt^{4+} ions replaced Mg^{2+} ions of the top layer of the MgO surface, while Mo^{6+} ions located on the surface in a distorted octahedral symmetry. The dehydrogenation activity of the $[PtMo_6]/MgO$ catalyst for the dehydrogenation reactions of butane, isobutane and propane was much higher compared to those of conventionally prepared bimetallic (Pt–Mo/MgO) and monometallic (Pt/MgO and Mo/MgO) catalysts. The selectivity to the corresponding alkenes was typically above 97%. The $[PtMo_6]/MgO$ ensemble catalyst was found to be resistant to deactivation due to coke formation.

Keywords: Characterization; Platinum; Molybdenum; Magnesium; Alkanes; Dehydrogenation

1. Introduction

Dehydrogenation of light alkanes towards more reactive unsaturated alkenes is a matter of increasing interest in petrochemical industry. The increasing demand for light alkenes, especially propene for polymerization and isobutene for gasoline blending, has lately stimulated research for developing dehydrogenation catalysts with improved catalytic performance. Furthermore, dehydrogenation reactions also serve as target reactions for fundamental research to examine and compare the catalytic performance of novel catalysts.

There are several limitations characterizing dehydrogenations which arise from the thermodynamics and kinetics of the reactions. Dehydrogenation reactions are endothermic and therefore run at moderate temperatures usually in the presence of added hydrogen to diminish the concentration of the more unsaturated precursors of 'coke'. As in all equilibrium limited reactions the maximum conversion that can be attained depends on the selected experimental parameters such as temperature, outlet pressure and inlet composition. To attain reasonable

* Corresponding author. Fax: (+81-3)58006892.

[1] Present address: Institute of Chemical Engineering and High Temperature Chemical Processes, University of Patras, Patras GR 26500, Greece.

[2] Department of Applied Chemistry, National Fisheries University of Pusan, Namku, Pusan 608-737, Korea.

PII S1381-1169(96)00117-3

yields in dehydrogenation reactions, one must work at elevated temperatures. Temperatures for 50% conversion at a total pressure of 1 atm are, for ethane, 998 K; for propane, n-butane and higher unbranched paraffins, 873 K, and for isobutane, 813 K [1]. The corresponding temperature for the conversion of 1-butene to butadiene is 933 K and for ethylbenzene to styrene, 893 K. The above temperatures required to give 50% conversion are lowered by about 100 K if the total pressure is 0.1 atm rather than 1 atm [1]. The position of equilibrium is favored by low partial pressures for selective hydrogenation and dehydrogenation. A simple way to overcome equilibrium limitations is by removing the product hydrogen, shifting the reaction towards dehydrogenated products. This can be accomplished using oxygen originating either from the gas phase or from an oxide surface. Hydrogen is removed as water by reaction with oxygen, making the reaction exothermic and irreversible. The use of ceramic membrane reactors is also being successfully used in dehydrogenation reactions to overcome the thermodynamic limitations by removing hydrogen. This promising method has extensively been studied and several suitable membranes permeable for hydrogen have been prepared and successfully tested [2,3].

The most desirable property of catalysts used in dehydrogenation reactions is probably resistivity against deactivation due to coke formation. The high temperatures required for the dehydrogenation reactions are such that, if a metallic catalyst is employed, considerable cracking to carbon with consequent loss of activity will rapidly occur. Platinum and other transition metal surfaces are covered with near monolayer of carbonaceous species during catalytic conversion reactions with hydrocarbons. Commercial dehydrogenation processes, therefore, use oxide catalysts instead, particularly those containing chromia. Cracking is less marked on oxides than on metals, and they are readily regenerated by oxidation. However, the chromium-containing oxide catalysts should be improved from toxic points of view. Recently, the $ZnAlO_x$ thin film catalysts showed higher activity and selectivity than the corresponding bulk catalysts [4].

In dehydrogenation reactions the catalytic performance depends not only on the thermodynamic factor but also on the mechanistic factor which determines the extent to which the adsorbed intermediate species undergo further reaction or desorb to give products. Surface geometry also affects the activity of catalysts. The species involved in the rate determining step of a catalytic dehydrogenation reaction may acquire one surface atom, ensembles of several adjacent surface atoms, or special surface atoms with a specific coordination number. When multiple surface-atom sites are required, the catalytic activity is often extremely sensitive to changes in surface structure and composition. For these reactions the use of specially prepared catalysts with well defined surface geometry is needed to improve catalytic performance.

The use of bimetallic catalysts in hydrocarbon reactions have extensively been studied because increased activity, selectivity and stability of the catalysts can be attained with the addition of a second metal [5]. The disadvantage of studying catalytic phenomena on bimetallic catalysts prepared by a conventional coimpregnation method is that the catalyst surfaces are often heterogeneous, which makes it difficult to explore their characteristics and further develop the catalytic systems. The use of bimetallic clusters as precursors has great advantages for preparation of relatively uniform bimetallic reaction sites well dispersed on support surfaces.

In the present study we have used a well defined inorganic cluster (hexamolybdoplatinate(IV) heteropolyanion) as a bimetal ensemble precursor, which has a plane Anderson structure [6]. The cluster precursor led to preparation of unique catalytic sites by reduction of the incipient supported clusters on Al_2O_3, which were active for hydrogenolysis reactions [7,8]. Our preliminary study demonstrated that the $[PtMo_6]/MgO$ catalyst prepared by using the hexamolybdoplatinate(IV) cluster, followed by

calcination at 773 K, showed a unique surface structure and better catalytic performance for the alkane-to-alkene conversion than a conventional coimpregnation catalyst. Here, we report a systematic characterization of the catalysts by X-ray absorption fine structure (XAFS) and the performance for the dehydrogenation reactions of propane, butane and isobutane.

2. Experimental

2.1. Catalyst preparation

The MgO-supported Pt–Mo bimetallic ensemble catalyst (denoted as $[PtMo_6]/MgO$) was prepared by an impregnation method using an aqueous solution of $(NH_4)_4[H_4PtMo_6O_{24}]$ with a plane structure composed of a central Pt(IV) ion and six octahedral molybdates as shown in Fig. 1 [6–8]. A catalyst with the same Pt–Mo composition was also prepared by a coimpregnation method using an aqueous solution of chloroplatinic acid and ammonium heptamolybdate (denoted as Pt–Mo/MgO). For comparison, monometallic catalysts, Pt/MgO, Mo/MgO and Pt/Al_2O_3, were also prepared. To examine the possible influence induced by the presence of residual chlorine on the catalyst surfaces, Cl-free Pt/MgO and Cl-free Pt–Mo/MgO catalysts were also prepared by using $Pt(C_5H_7O_2)_2$ and/or $(NH_4)_6[Mo_7O_{24}]$. Chlorine-free Pt/MgO was prepared by impregnation of MgO with an acetone solution of $Pt(C_5H_7O_2)_2$ followed by evaporation at 318 K and drying at 348 K for 24 h. The resultant catalyst was then used to prepare Cl-free Pt–Mo/MgO by impregnation with an aqueous solution of $(NH_4)_6[Mo_7O_{24}]$ followed by evaporation at 363 K and drying at 393 K for 24 h. The metal loading was the same for all catalysts (1 wt% for Pt and 3 wt% for Mo). The MgO employed as support was prepared by calcina-

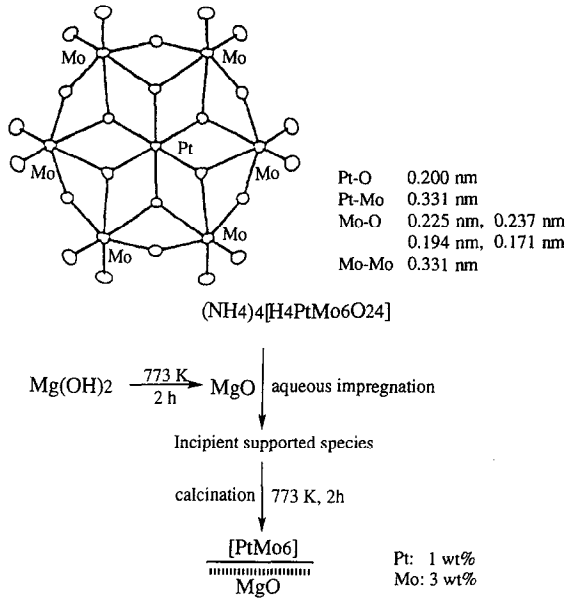

Fig. 1. Preparation procedure for the $[PtMo_6]/MgO$ catalyst by using $[PtMo_6O_{24}]^{8-}$ heteropolyanion.

Table 1
Catalysts and probe reactions employed in the present study

Catalyst	Precursor	Probe reaction		
		isobutane	butane	propane
		Reaction temperature (K)		
$[PtMo_6]/MgO$	$(NH_4)_4[H_4PtMo_6O_{24}]$	573–773	573–773	573–773
Pt–Mo/MgO	$H_2PtCl_6 + (NH_4)_6Mo_7O_{24}$	573–773	573–773	573–773
Pt/MgO	H_2PtCl_6	573–773	573–773	573–773
Mo/MgO	$(NH_4)_6Mo_7O_{24}$	573–773	573–773	573–773
Pt/Al_2O_3	H_2PtCl_6	573–773	573–773	573–773
Pt/MgO (Cl-free)	$Pt(C_5H_7O_2)_2$ [a]	723, 773	–	673–773
Pt-Mo/MgO (Cl-free)	$Pt(C_5H_7O_2)_2$ [a] + $(NH_4)_6Mo_7O_{24}$	623, 723, 773	–	–

Metal loading: 1 wt% Pt, 3 wt% Mo; pretreatment: oxidation at 773 K for 2 h.
[a] Solvent is acetone, while water for others.

tion of $Mg(OH)_2$ at 773 K for 2 h. In Table 1 are listed all catalysts prepared, the precursors used and the probe reactions employed to test their catalytic performance.

2.2. EXAFS measurements

Structures of the bimetallic and monometallic catalysts at each stage of preparation, pretreatment and reaction were examined by means of EXAFS. Spectra of the $[PtMo_6O_{24}]^{8-}$ precursor were also obtained. EXAFS spectra of the $[PtMo_6]$/MgO and Pt–Mo/MgO samples after impregnation as well as after calcination at various temperatures between 423 and 773 K were obtained in order to examine the extent of the interaction between the precursor and the support upon increasing calcination temperature. The samples were calcined in a closed circulating system under an oxygen pressure of 13.3 kPa. The $[PtMo_6]$/MgO and Pt–Mo/MgO catalysts were also examined after propane dehydrogenation at 573 and 723 K for 4 h, while the structure of the ensemble catalyst after reduction with hydrogen at 773 K for 2 h was also studied. After these treatments the samples were transferred to glass EXAFS cells with Kapton windows without contacting air.

The Pt L_{III}-edge and Mo K-edge EXAFS spectra were obtained in a transmission mode at the BL-7C and BL-10B stations of the Photon Factory in the National Laboratory for High Energy Physics (Proposal No 92001), using Si(311) or Si(111) monochromators. The optical length of the EXAFS cells was 10 mm for the Pt L_{III}-edge and 5 mm for the Mo K-edge measurements. EXAFS spectra were obtained at 298 K and analysed using the EXAFS analysis program EXAFSH [9]. The analysis involves pre-edge extrapolation, background removal using a cubic spline method, Fourier transformation using a Hanning window function, inverse Fourier transformation and curve fitting. The Fourier transformation range used was 30–130 nm^{-1} for the Pt L_{III}-edge and 35–145 nm^{-1} for the Mo K-edge. The amplitude and phase shift functions for the Pt–Pt, Mo–O and Mo–Mo bonds were extracted from the EXAFS spectra at 298 K obtained from Pt foil, K_2MoO_4 and Mo foil, respectively. The corresponding functions for the Pt–O, Pt–Mg and Mo–Mg bonds were theoretically calculated using the FEFF5 program [10–12].

2.3. Catalytic performance

The catalytic performance of the samples was examined in a fixed-bed flow reactor. It consists of a flow measuring and control system, the reactor and an on-line analytical system. Flow rates of high purity N_2, O_2 and alkanes were measured and controlled using flow meters and needle valves. The reactor is a 30 cm long Pyrex tube with an expanded 2 cm long section in the middle (8 mm I.D.) in which the catalyst sample was placed by means of quartz-wool pieces. The furnace temperature was controlled by a temperature controller using a K-type thermocouple placed between the reactor and the walls of the furnace. Reaction temperature was measured inside the catalyst bed by a K-type thermocouple (0.5 mm O.D.) placed in a 1/16 in. O.D. stainless steel well which runs through the center of the cell. The outlet of the reactor was connected to a GC equipped with a thermal conductivity detector. Reaction products were separated using a VZ10 or a VZ7 column.

Catalytic performance was studied using dehydrogenation of propane, butane and isobutane as probe reactions in the temperature range 573–773 K. In all experiments reported here the pure alkane at atmospheric pressure was used in the feed. The flow rates were 20 cm^3/min for isobutane, 15 cm^3/min for butane, and 18 cm^3/min for propane.

In a typical experiment 300 mg of a catalyst in a powder form was placed in the Pyrex reactor. The sample was then slowly heated to 773 K under flowing nitrogen and calcined at the same temperature for 2 h under a flowing O_2–N_2 mixture. After flushing with nitrogen to remove gas phase oxygen from the reactor the

sample was cooled down to the lowest examined reaction temperature. A flow of the reactant alkane was then measured through a loop bypass and the alkane was introduced to the catalyst by means of two 3-way valves. The product distribution at the effluent of the reactor was recorded every 20–30 min for approximately 5 h. After the completion of a reaction run the catalyst was again heated at 773 K under an O_2–N_2 mixture and the next reaction run at a higher reaction temperature was conducted.

'Blank' experiments showed that the Pyrex reactor, the quartz wool pieces and the stainless steel thermocouple did not affect at any measurable extent the kinetic measurements. Representative experiments were repeated to confirm the reproducibility of the results.

3. Results and discussion

3.1. Catalytic activity and selectivity

3.1.1. Butane dehydrogenation

Performance of the $[PtMo_6]/MgO$ catalyst for butane dehydrogenation as a target reaction was studied in the temperature range 573–773 K and compared with that of conventionally prepared bimetallic and monometallic catalysts. The yield and selectivity to butenes over $[PtMo_6]/MgO$ as a function of time-on-stream are shown in Fig. 2(a) and 2(b), respectively, where the yield and the selectivity are defined as [produced butenes]/[fed butane] and [produced butenes]/[consumed butane], respectively. It was observed that the yield was initially high but gradually decreased with time-on-stream. The decrease of yield was more pronounced at reaction temperatures above 723 K, particularly at 773 K where deactivation of the catalyst was rapid and the catalytic activity nearly ceased a few hours after introducing butane over the catalyst. The selectivity initially increased with time-on-stream and reached a constant value, typically about 98% after 2–3 h

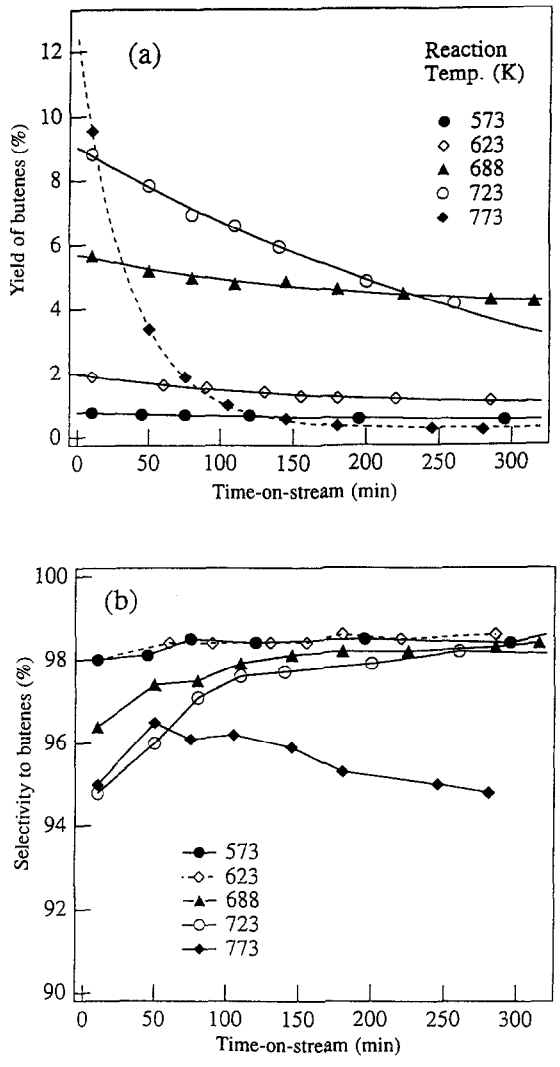

Fig. 2. Yield (a) and selectivity (b) to butenes as a function of time-on-stream for the $[PtMo_6]/MgO$ catalyst in the temperature range 573–773 K. Cat. weight: 0.3 g; Flow rate: 15 cm^3 butane/min.

in operation except the reaction at 773 K, where almost complete deactivation of the catalyst occurred (Fig. 2(b)). No butadiene was produced under the present conditions and byproducts were small amounts of C_1–C_3 hydrocarbons.

Similar experiments were conducted with the co-impregnated Pt–Mo/MgO catalyst. Results of the yield and the selectivity of Pt–Mo/MgO as a function of time-on-stream are shown in Fig. 3(a) and 3(b), respectively. Not only the yields in the initial stage of reaction were much

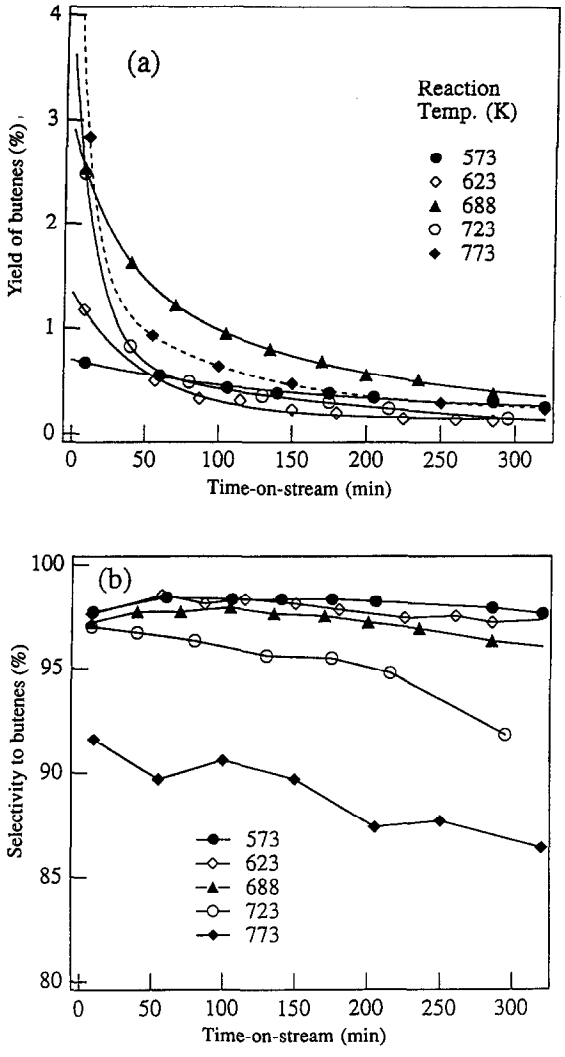

Fig. 3. Yield (a) and selectivity (b) to butenes as a function of time-on-stream for the Pt–Mo/MgO catalyst in the temperature range 573–773 K. Cat. weight: 0.3 g; Flow rate: 15 cm^3 butane/min.

lower than those for the $[PtMo_6]/MgO$ catalyst, but also deactivation was more rapid at all reaction temperatures (Fig. 3(b)). The selectivity to butenes dropped to lower values at temperatures above 723 K (Fig. 3(b)). Small amounts of butadiene were produced on Pt–Mo/MgO above 723 K. Pt/MgO and Mo/MgO were almost inactive under the present conditions.

The superiority of the $[PtMo_6]/MgO$ catalyst is more pronounced upon comparing deactivation rate of the catalysts at any reaction temperature. The $[PtMo_6]/MgO$ catalyst not only exhibits a higher yield, but also deactivates more slowly compared to the Pt–Mo/MgO catalyst. As a result, after 3–4 h time-on-stream the butene yield over the ensemble catalyst is about one order of magnitude higher than that for the conventionally prepared catalyst.

3.1.2. Propane dehydrogenation

The catalytic performance of $[PtMo_6]/MgO$ was also examined in the propane dehydrogenation reaction in Fig. 4, which shows the yield (a) and selectivity (b) to propene as a function of time-on-stream. The yield and the selectivity are defined as produced propene/fed propane and produced propene/consumed propane, respectively. For this reaction, deactivation was not so fast as in the case of butane dehydrogenation. At reaction temperatures up to 723 K there was no significant decrease in the catalytic activity and slow deactivation occurred only at 773 K as shown in Fig. 4(a). Selectivity to propene increased during the first two hours of the reaction and reached a constant value, typically above 96% for the rest of the reaction (Fig. 4(b)).

Activity of the conventionally prepared Pt–Mo/MgO catalyst for the propane dehydrogenation was not so good as that of the $[PtMo_6]/MgO$ catalyst. The catalytic performance of Pt/Al_2O_3 was comparable to the Pt–Mo/MgO catalyst, exhibiting similar steady-state selectivities, while deactivation of Pt/Al_2O_3 was more serious. The monometallic Pt/MgO and Mo/MgO catalysts were almost inactive under the similar conditions. Generally, the difference between the ensemble catalyst and the rest of catalysts became more pronounced at high reaction temperatures.

3.1.3. Isobutane dehydrogenation

The complete set of the catalysts listed in Table 1 was studied for isobutane dehydrogenation in the temperature range 573–773 K. In Fig. 5 is shown the yield (a) and selectivity (b) to isobutene (defined as produced isobutene/fed

isobutane and produced isobutene/consumed isobutane, respectively) as a function of time-on-stream on the $[PtMo_6]/MgO$ catalyst. It was observed that the isobutene yield remained constant with time-on-stream at reaction temperatures up to 723 K and only at 773 K a gradual decrease in the yield with time took place, possibly indicating that at this temperature deactivation due to coke formation became important. Selectivity to isobutene showed no decrease during the period of reaction examined

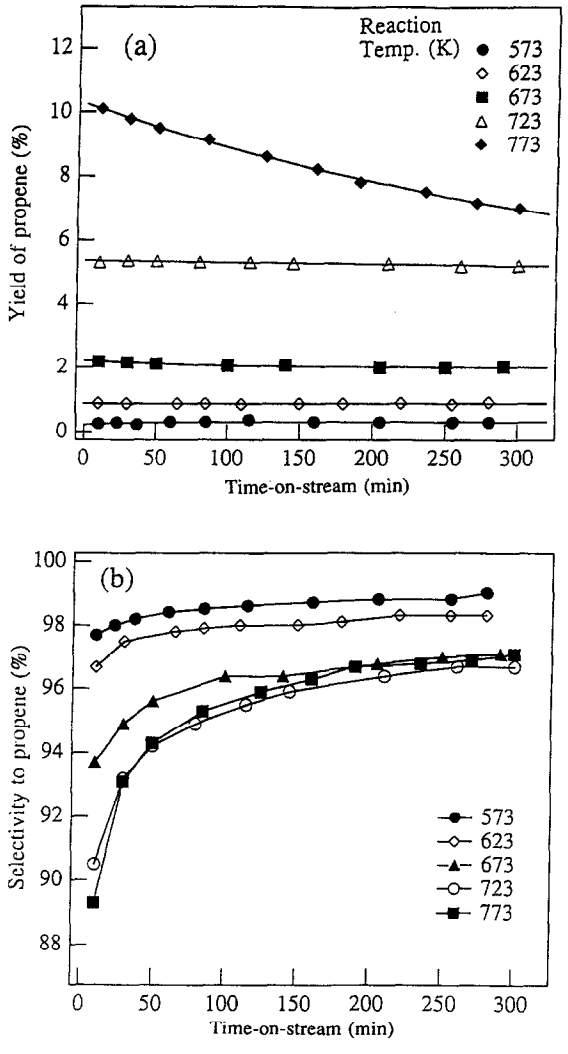

Fig. 4. Yield (a) and selectivity (b) to propene as a function of time-on-stream for the $[PtMo_6]/MgO$ catalyst, in the temperature range 573–773 K. Cat. weight: 0.3 g; Flow rate: 18 cm^3 propane/min.

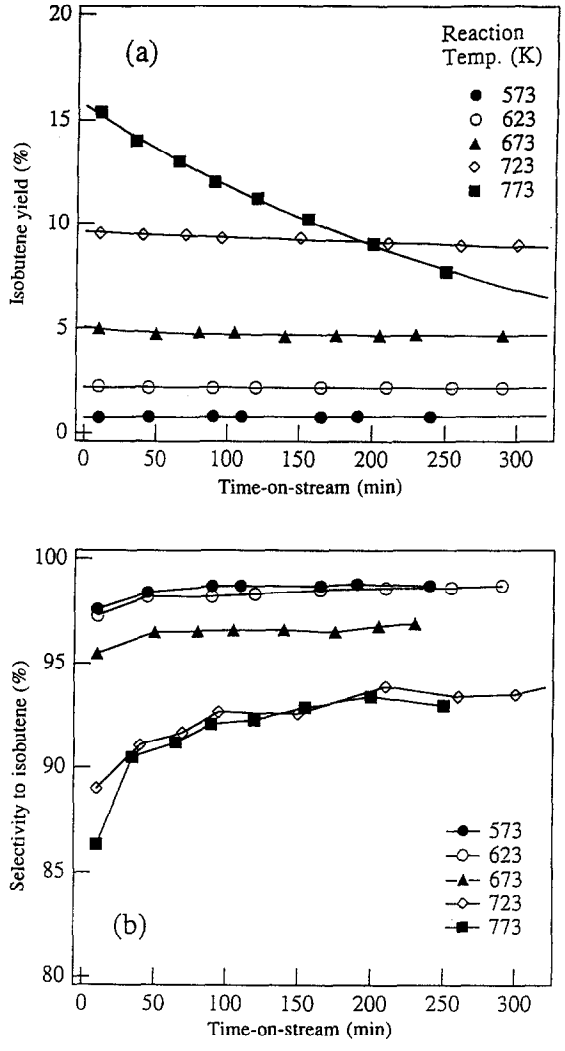

Fig. 5. Yield (a) and selectivity (b) to isobutene as a function of time-on-stream for the $[PtMo_6]/MgO$ catalyst in the temperature range 573–773 K. Cat. weight: 0.3 g; Flow rate: 20 cm^3 isobutane/min.

(Fig. 5(b)). Byproducts of the reaction were C_1–C_3 hydrocarbons.

Similar experiments were conducted with the conventionally prepared Pt–Mo/MgO catalysts. The catalytic activity of Pt–Mo/MgO was much lower than that of the ensemble catalyst and the selectivity to isobutene had a decreasing trend with time-on-stream, especially at high reaction temperatures. It is to be noted that the high deactivation rates were observed on the Pt–

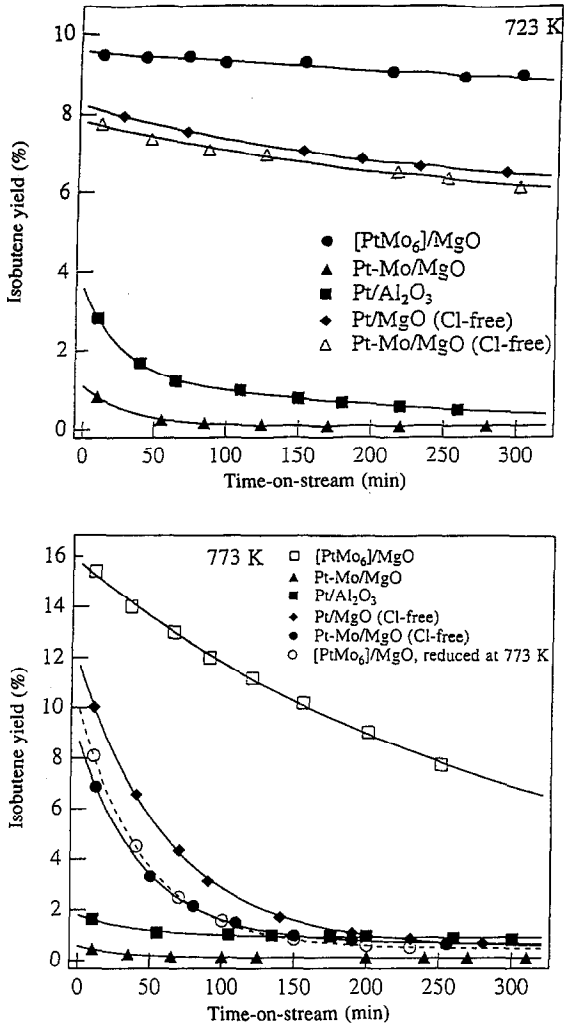

Fig. 6. Yield of isobutene at 723 (a) and 773 K (b) as a function of time-on-stream for the various catalysts. The isobutene yield at 773 K on $[PtMo_6]/MgO$ reduced with H_2 at 773 K for 2 h as a function of time-on-stream is also shown.

Mo/MgO catalyst at all reaction temperatures, and even at 573 K.

Comparisons of various catalysts in the isobutene yields as a function of time-on-stream at 723 and 773 K are shown in Fig. 6. The superiority of the $[PtMo_6]/MgO$ catalyst to the PtMo/MgO catalyst is evident. The Pt/Al_2O_3 catalyst also showed a lower activity with a rapid deactivation. To examine the effect of the residual chlorine that may be present on the conventionally prepared catalysts, isobutane dehydrogenation reactions at 723 and 773 K were also carried out on Cl-free Pt–Mo/MgO and Cl-free Pt/MgO catalysts. The Cl-free samples exhibited a much better catalytic performance compared to the residual chlorine-containing Pt–Mo/MgO catalyst at 723 K (Fig. 6(a)), but they were rapidly deactivated at 773 K as shown in Fig. 6(b). As consequence, the Cl-free Pt–Mo/MgO and Cl-free Pt/MgO catalysts were not so good as the $[PtMo_6]/MgO$ ensemble catalyst. It is to be noted that when the activity of the Cl-free Pt/MgO catalyst decreased by coexistence with Mo oxides in the Cl-free Pt–Mo/MgO catalyst, whereas the ensemble catalyst exhibited the best catalytic performance, regarding activity and resistivity to deactivation.

As mentioned in the Section 2.2., EXAFS analysis shows that platinum atoms in the $[PtMo_6]/MgO$ catalyst are reduced during the reaction at 723 K. In order to examine the effect of this factor on the catalytic performance of $[PtMo_6]/MgO$, the catalyst was deeply reduced in flowing H_2 (40 cm^3/min) at 773 K for 2 h. After this treatment the activity of the catalyst was significantly lowered as shown in Fig. 6(b). After reduction of the sample at 773 K, the initial yield of isobutene (extrapolated to $t = 0$ by exponential fitting) was about two thirds of that of the unreduced catalyst, but most importantly, deactivation on the reduced catalyst occurred much faster. On the contrary, the treatment of the Cl-free Pt–Mo/MgO catalyst with H_2 at 773 K for 2 h did not change the catalytic performance. Calcination of the reduced $[PtMo_6]/MgO$ sample in air at 773 K for 2 h restored neither the activity of the sample nor the deactivation property. It seems that this high temperature treatment with hydrogen destroyed the specific structure of the $[PtMo_6]/MgO$ ensemble catalyst to become similar to that of the conventionally prepared catalyst.

3.1.4. Catalyst stability

It was found that the novel $[PtMo_6]/MgO$ catalyst was more active and selective for butane, isobutane and propane dehydrogenation

reactions, and most importantly, resistant to deactivation due to coke formation as compared to the rest of the examined catalysts as shown in Figs. 2–6. The observed difference in the catalytic performance seems to be related to the difference in the properties of the catalyst surfaces that originates from the variations of the preparation methods.

The enhanced capability of the $[PtMo_6]/MgO$ ensemble catalyst to resist deactivation, as compared to the other catalysts, is one of the interesting results in this study. This property of the $[PtMo_6]/MgO$ catalyst may arise either (i) from its ability to inhibit the formation of coke precursors or (ii) from the existence of a process capable for maintaining the catalytically active sites free from coke. Starting from the second possibility, it is well known that the addition of the second metal to platinum-containing bimetallic catalysts usually enhances the catalyst stability. It was reported for the Pt–Sn catalysts that 30% of the metal surface remain uncovered in the steady state, whereas for the Pt catalyst this fraction only remains at 10%. It was also reported that the addition of a second component to Pt/Al_2O_3 catalyst gave rise to more mobile coke precursors. This hypothesis of increased mobility of surface intermediates to the support might also be valid in the case of the $[PtMo_6]/MgO$ catalyst, but would not be adequate to explain the large difference in the deactivation profile between the ensemble catalyst and the conventionally prepared Pt–Mo/MgO catalyst (Figs. 2–6). It is more probable that the difference arises from the inhibition of coke formation over $[PtMo_6]/MgO$ due to its specific surface structure. It is believed that alkane dehydrogenation over metals is structure insensitive and does not require a large ensemble of neighboring atoms. On the other hand, coke deposition involves larger ensembles of atoms as active sites. On the catalysts prepared by the $[PtMo_6O_{24}]^{8-}$ cluster precursor with a plane structure of a Pt atom isolated by surrounding six molybdates, a geometric restriction would diminish coke formation without affecting significantly the activity towards dehydrogenation.

The presence of acid sites on the support is undesirable in dehydrogenations since they catalyze side reactions. It should be recalled that the acidic character of chlorine favors cleavage of the C–C bonds, deep dehydrogenation, and polymerization processes that lead to carbon deposition and, consequently, faster deactivation and decreased activity, selectivity and stability of the catalysts [4]. It was observed that Cl-containing Pt/MgO is more active for hydrogenolysis, that involves cleavage of a C–C bond, than the Cl-free samples. The rapid deactivation of the Cl-containing catalysts in the present study could, therefore, be partly attributed to the presence of chlorine ions on the catalysts which favor carbon deposition and subsequent deactivation of the catalysts. The increase in selectivity observed in the beginning of the reaction runs (e.g. Fig. 2, Figs. 4 and 5(b)) was more pronounced at high reaction temperatures, which may be attributed to the presence of different active sites on the fresh catalyst. Another possible explanation may be the gradual change of the averaged oxidation state of the platinum atoms during the reaction. The EXAFS analysis (in Section 2.2.) revealed that Pt atoms were reduced with time-on-stream to form small particles under the reaction conditions. If selectivity is higher over the Pt particles thus obtained, the increasing trend of selectivity with time-on-stream could be attributed to this process. To obtain the information of the structures of the bimetallic catalysts, we performed the EXAFS experiments under various conditions.

3.2. Catalyst characterization

3.2.1. $[PtMo_6]/MgO$ catalyst

3.2.1.1. Effect of calcination temperature on the structures around Pt and Mo atoms. The structure of the novel $[PtMo_6]/MgO$ ensemble catalyst was determined by EXAFS after supporting the $[PtMo_6O_{24}]^{8-}$ precursor on MgO and after

calcination with oxygen at various temperatures in the range 423–773 K. Analysis of the EXAFS spectra for the incipient supported sample revealed that the framework of the $[PtMo_6O_{24}]^{8-}$ precursor was destroyed upon impregnation. The characteristic Pt–Mo bond of the precursor was not observed and the analysis of the Pt L_{III}-edge and Mo K-edge EXAFS spectra showed the existence of only Pt–O (0.200 nm) bond or Mo–O (0.175 nm) bond as shown in Table 2. The incipient supported sample was calcined under oxygen for 2 h at 423, 573, 673 and 773 K. EXAFS spectra for the treated samples were measured to determine structural changes and to observe the extent of interaction (bonding modes) between the heteropolyanion precursor with a plane structure and the MgO support upon increasing calcination temperature. The EXAFS analysis results are listed in Table 2. For the sample calcined at 423 K there was no particular interaction between the precursor and the support observable by EXAFS (Table 2). Calcination above 573 K led to the appearance of Pt–Mg (0.302 nm) and 'long' Pt–O (0.360 nm) bonds besides Pt–O bond at 0.202 nm. Around Mo atoms there only

Table 2
Curve fitting results of the Pt L_{III}-edge and Mo K-edge EXAFS spectra for the $[PtMo_6]$/MgO catalyst after impregnation and calcination under oxygen in the temperature range 423–773 K

	Bond	N [a]	R [b] (nm)	ΔE_0 [c] (eV)	σ [d] (nm)	R factor [e] (%)
$[PtMo_6O_{24}]^{8-}$ precursor	Pt–O	6.0	0.199	10.1	0.0055	
	Pt–Mo	4.0	0.329	0.5	0.0085	1.4
	Mo–O	4.5	0.175	−3.5	0.0075	
	Mo–Pt	1.0	0.330	−4.7	0.0072	1.2
	Mo–Mo	2.0	0.334	−1.3	0.0061	
Incipient supported species	Pt–O	6.7	0.200	10.5	0.0058	1.2
	Mo–O	4.5	0.175	−3.5	0.0075	4.0
Calcination at 423 K	Pt–O	6.5	0.200	10.4	0.0059	1.2
	Mo–O	4.6	0.175	−3.4	0.0076	3.6
Calcination at 573 K	Pt–O	6.5	0.202	10.9	0.0064	
	Pt–Mg	4.6	0.305	8.9	0.0090	0.2
	Pt–O	6.2	0.361	−0.9	0.0083	
	Mo–O	3.9	0.176	−3.8	0.0075	4.0
Calcination at 673 K	Pt–O	6.3	0.202	10.8	0.0065	
	Pt–Mg	6.5	0.302	7.7	0.0090	0.2
	Pt–O	7.3	0.360	−1.4	0.0083	
	Mo–O	2.3	0.174	−11.8	0.0071	
	Mo–Mg	2.0	0.279	8.0	0.0085	3.6
Calcination at 773 K	Pt–O	6.2 ± 1.0	0.202 ± 0.001	10.6 ± 3.0	0.0064 ± 0.0010	
	Pt–Mg	8.1 ± 1.3	0.302 ± 0.001	7.4 ± 3.0	0.0093 ± 0.0010	0.6
	Pt–O	4.8 ± 0.9	0.360 ± 0.001	−2.1 ± 3.0	0.0064 ± 0.0010	
	Mo–O	1.6 ± 0.4	0.174 ± 0.001	−7.1 ± 4.0	0.0059 ± 0.0011	
	Mo–Mg	3.0 ± 0.7	0.282 ± 0.001	15.0 ± 4.0	0.0102 ± 0.0011	2.5
	Pt–O *	6.1	0.202	9.8	0.0064	
	Pt–Mg *	14.1	0.305	10.0	0.0127	2.3

[a] Coordination number.
[b] Bond distance.
[c] The energy difference between the origins of the photoelectron wave vector.
[d] Debye–Waller factor.
[e] Residual factor; Fourier transform range: 30–130 nm^{-1} for Pt L_{III}-edge and 35–145 nm^{-1} for Mo K-edge; Fourier filtering range: 0.10–0.35 nm^{-1} for Pt L_{III}-edge and 0.10–0.30 nm^{-1} for Mo K-edge. * Two-wave fitting analysis shown for comparison.

existed Mo–O bonds at 0.175 nm for the samples calcined at 423–573 K. Above 673 K Mo–Mg (0.279–0.282 nm) bonds were also observed. The intensity of the k^3-weighted Fourier transformed EXAFS peaks for Pt–Mg and Mo–Mg bonds increased upon increasing calcination temperature from 573 to 773 K, indicating stronger interaction between Pt and Mo atoms and the support.

A representative set of the EXAFS data is shown in Fig. 7, where the Pt L_{III}-edge EXAFS raw data, the extracted oscillation and the associated Fourier transform and the curve fitting results for the $[PtMo_6]/MgO$ catalyst calcined at 773 K are presented. We performed the detailed EXAFS analysis by a curve fitting technique as follows. At first, the peak around 0.3 nm in the Fourier transform was analyzed by assuming it as Pt–Mo bonding as in the precursor structure, but it was entirely different. Rather, this peak seemed to be fitted as Pt–Mg. Then we performed the EXAFS analysis over a whole Fourier range 0.1–0.35 nm by two-wave (Pt–O and Pt–Mg) fitting as shown in Fig. 7(d). However, the oscillation particularly in the higher energy region was not reproduced (Fig. 7(d)). The coordination number of Pt–Mg bond was determined to be 14.1 in Table 2 (bottom column) which is an unrealistic value and the Debye–Waller factor of 0.0127 nm is fairly

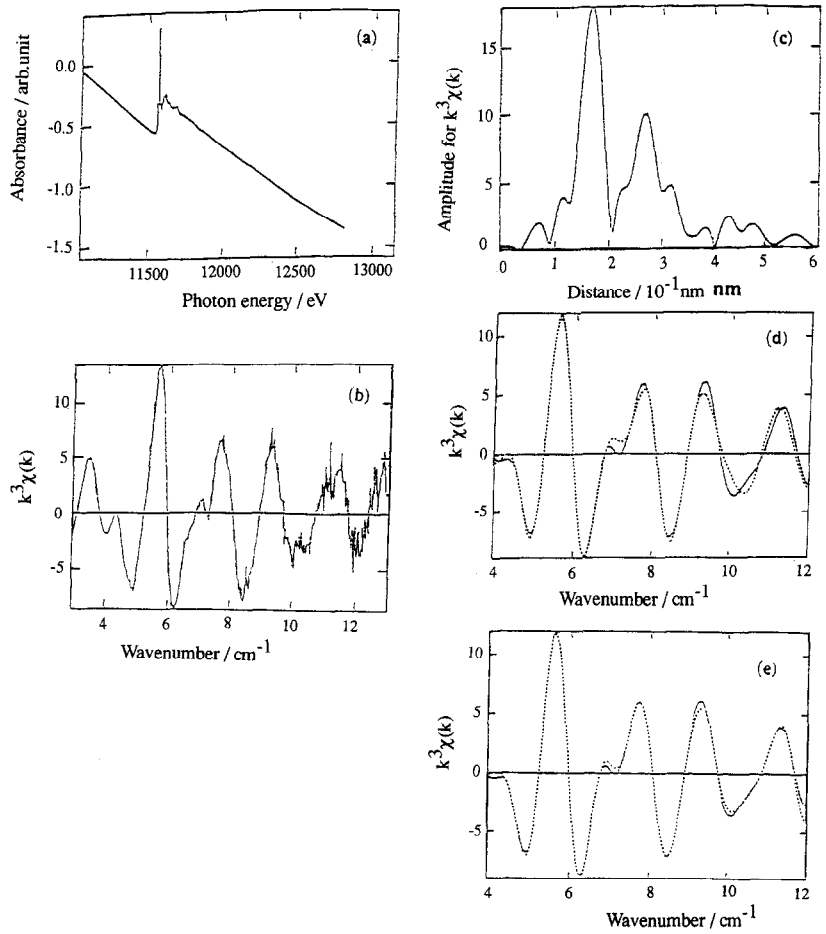

Fig. 7. Pt L_{III}-edge EXAFS data for the $[PtMo_6]/MgO$ catalyst after calcination at 773 K for 2 h; (a) raw data, (b) k^3-weighted $\chi(k)$, (c) Fourier transform (Fourier transform range: 30–130 nm), (d) curve fitting using Pt–O + Pt–Mg, and (e) curve fitting using Pt–O + Pt–Mg + Pt–O. Fourier filtering range: 0.1–0.35 nm.

large as shown in Table 2. Since the appearance of Pt–Mg bond implies the incorporation of Pt atoms to the MgO lattice or at least strong interaction of Pt atoms with the MgO lattice, we took into account the longer Pt–O bond expected from the MgO rock-salt structure and analyzed the EXAFS data by three-wave (Pt–O, Pt–Mg and Pt–O (long)) fitting. This analysis well reproduced the observed data as shown in Fig. 7(e). The best fit results are shown in Table 2, where the bond distances and coordination numbers of Pt–O, Pt–Mg and Pt–O (long) were determined to be 0.202 nm and 6.2, 0.302 nm and 8.1, and 0.360 nm and 4.8, respectively.

Mo K-edge EXAFS Fourier transform for the $[PtMo_6]/MgO$ catalyst calcined at 773 K is shown in Fig. 8(a). Assuming the first and second peaks as Mo–O and Mo–Mg bonds, respectively, two-wave (Mo–O + Mo–Mg) fitting reproduced the observed data as shown in Table 2. Attempts to fit the Mo K-edge EXAFS oscillation by bonds other than those listed in Table 2 did not give any good fitting result.

The oxidation state of the platinum ions can be estimated by comparing the 'white line' intensity of the Pt L_{III}-edge spectra, which is related to the d-electron vacancy of Pt atom [13–16], with that of the $[PtMo_6O_{24}]^{8-}$ precursor with a known oxidation state of platinum atoms (Pt^{4+}). The Pt L_{III}-edge 'white line' intensity of the $[PtMo_6]/MgO$ catalyst in Fig. 7(a) was found to be almost the same as that for the Pt (IV) atoms of the $[PtMo_6O_{24}]^{8-}$ precursor, taking into account the height of edge jump

Table 3
Comparison of the local structure of Pt atoms of the $[PtMo_6]/MgO$ catalyst after calcination at 773 K with that of Mg atoms in MgO

	Bond	Bond length (nm)	Coordination number	
$[PtMo_6]/MgO$	Pt–O	0.202 ± 0.001	6.2 ± 1.0	5 [a]
	Pt–Mg	0.302 ± 0.001	8.1 ± 1.3	8 [a]
	Pt–O	0.360 ± 0.001	4.8 ± 0.9	4 [a]
MgO	Mg–O	0.210	6	
	Mg–Mg	0.297	12	
	Mg–O	0.364	8	

[a] Expected values from the Pt location at the surface top layer replacing Mg^{2+}.

for both samples. Thus the platinum atoms in the $[PtMo_6]/MgO$ ensemble catalyst seems to be in the 4 + state.

As can be seen from the data listed in Table 3, the bond lengths of Pt–O, Pt–Mg and Pt–O (long) for the $[PtMo_6]/MgO$ catalyst after calcination at 773 K are similar to the bond lengths of Mg–O, Mg–Mg and Mg–O of MgO crystal, respectively. This similarity of the bond lengths indicates that after calcination at 773 K platinum atoms substitute Mg^{2+} atoms in the lattice of the MgO support. The coordination numbers of Pt–Mg and Pt–O (long) bonds are, however, much smaller than the corresponding coordination numbers for MgO. MgO preferably has a (100) surface because it is the most stable surface of MgO [17]. If Pt atoms occupy Mg^{2+} sites at the first surface layer of the MgO, the coordination numbers for Pt–O, Pt–Mg and Pt–O bonds are expected to be 5, 8 and 4,

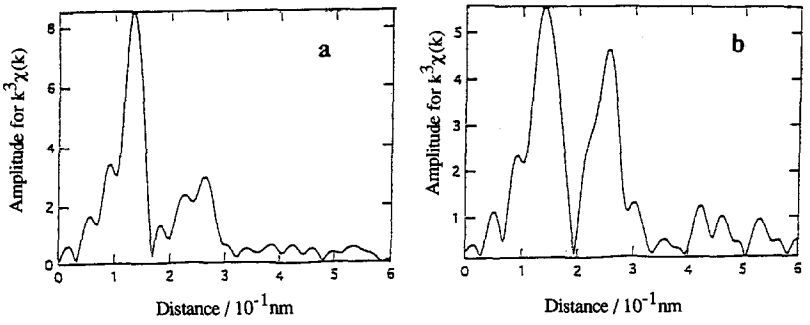

Fig. 8. Mo K-edge EXAFS Fourier transforms for $[PtMo_6]/MgO$ after calcination at 773 K (a) and propane dehydrogenation at 723 K (b).

respectively. These values are similar to the curve fitting results (Table 3). A local structure model for the Pt sites is illustrated in Fig. 9(a). The substitution model well explains the observed XAFS data, though a slight relaxation of the local structure around Pt ion.

Some representative Mo K-edge XANES spectra obtained from the examined catalysts in various conditions are shown in Fig. 10. The $[PtMo_6]/MgO$ catalyst exhibited a pre-edge peak which is attributed to a forbidden 1s → 4d bound-state transition [18]. It has been demonstrated that the intensity of this peak, which is more intense for tetrahedral symmetry (e.g. $MgMoO_4$), can be used as a measure of the number and shortness of the Mo–O bonds [18]. In our experiments, the intensity of the pre-edge peak of the $[PtMo_6]/MgO$ catalyst after calcination at 773 K was observed to be much smaller than that of $MgMoO_4$, indicating that in the calcined $[PtMo_6]/MgO$ catalyst the majority of Mo atoms have an octahedral coordination. This coincides with the results from detailed studies of a series of MoO_3/MgO samples using XANES [19] and Raman Spectroscopy [20] which showed that for the catalysts with Mo loading below 3.3 wt%, isolated, distorted octahedral Mo species are present on MgO after calcination at temperatures above 673 K. As shown in Table 2, however, the coordination number of Mo–O bond decreased with increasing calcination temperature and at 773 K had a value much smaller than the expected one from an octahedrally coordinated Mo^{6+} species, e.g. MoO_3 and $(NH_4)_6Mo_7O_{24}$ [21], suggesting the presence of some distortion on the Mo coordination sphere. When distorted

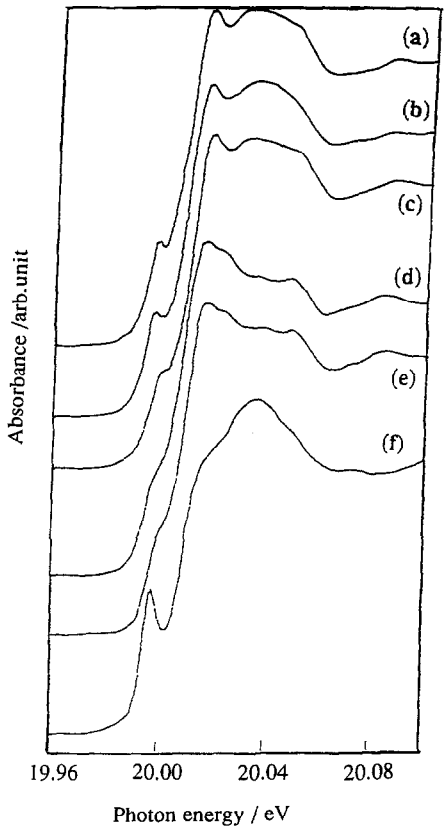

Fig. 10. Mo K-edge XANES spectra for the examined catalysts after treatments at various conditions; (a) $[PtMo_6]/MgO$ after calcination at 773 K, (b) Pt–Mo/MgO after calcination at 773 K, (c) Mo/MgO after calcination at 773 K, (d) Pt–Mo/MgO after propane dehydrogenation at 723 K, (e) $[PtMo_6]/MgO$ after propane dehydrogenation at 723 K, and (f) $MgMoO_4$ (Mo:tetrahedral).

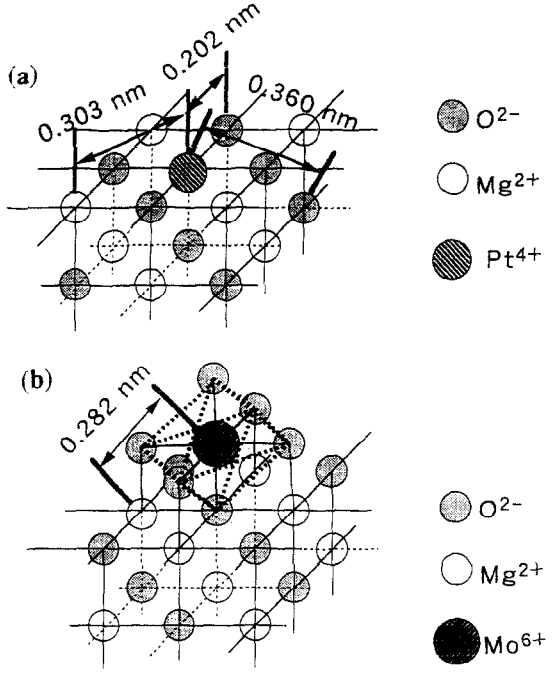

Fig. 9. Model structures of Pt (a) and Mo (b) atoms of the $PtMo_6]/MgO$ catalyst after calcination at 773 K.

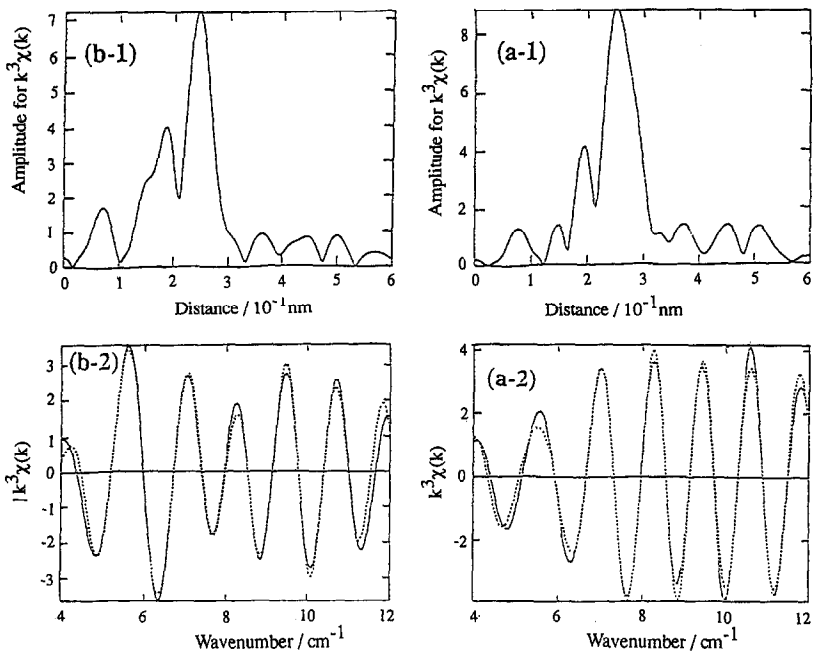

Fig. 11. Pt L_{III}-edge spectra for $[PtMo_6]/MgO$ after propane dehydrogenation reaction for 2 h at 723 K (a) and 573 K (b); (a-1) and (b-1): Fourier transform (Fourier transform range: 30–130 nm); (a-2): curve fitting of one wave (Pt–Pt), (b-2): curve fitting of three waves (Pt–O + Pt–Mg + Pt–Pt); Fourier filtering range: 0.16–0.32 nm.

Table 4
Curve fitting results of the Pt L_{III}-edge and Mo K-edge EXAFS spectra for the $[PtMo_6]/MgO$ catalyst after propane dehydrogenation reactions at 573 and 723 K and after reduction with hydrogen at 773 K

	Bond	N [a]	R [b] (nm)	ΔE_0 [c] (eV)	σ [d] (nm)	R factor [e] (%)
After C_3H_8 reaction at 573 K	Pt–O	1.1 ± 0.4	0.203 ± 0.001	8.9 ± 3.0	0.0064 ± 0.0011	
	Pt–Mg	2.4 ± 0.5	0.303 ± 0.001	8.1 ± 3.0	0.0086 ± 0.0011	3.6
	Pt–Pt	4.4 ± 0.9	0.273 ± 0.001	2.0 ± 3.0	0.0077 ± 0.0011	
	Mo–O	1.6 ± 0.4	0.175 ± 0.001	−0.3 ± 4.0	0.0060 ± 0.0012	4.0
	Mo–Mg	2.8 ± 0.7	0.280 ± 0.001	15.0 ± 4.0	0.0099 ± 0.0012	
After C_3H_8 reaction at 723 K	Pt–Pt	7.2 ± 1.3	0.274 ± 0.001	−2.1 ± 3.0	0.0083 ± 0.0011	2.9
	Mo–O	1.5 ± 0.4	0.177 ± 0.001	10.0 ± 4.0	0.0067 ± 0.0012	
	Mo–Mg	3.5 ± 0.7	0.285 ± 0.001	13.5 ± 4.0	0.0059 ± 0.0012	2.1
	Mo–Mo	1.5 ± 0.4	0.287 ± 0.001	−5.5 ± 4.0	0.0079 ± 0.0012	
After H_2 reduction at 773 K	Pt–Pt	6.8 ± 1.3	0.273 ± 0.001	−3.0 ± 3.0	0.0085 ± 0.0010	1.6
	Mo–O	4.1 ± 0.7	0.184 ± 0.001	20.1 ± 3.0	0.0100 ± 0.0011	
	Mo–Mg	6.6 ± 1.0	0.286 ± 0.001	15.2 ± 3.0	0.0050 ± 0.0011	1.5
	Mo–Mo	2.5 ± 0.5	0.288 ± 0.001	1.1 ± 3.0	0.0069 ± 0.0011	

[a] Coordination number.
[b] Bond distance.
[c] The energy difference between the origins of the photoelectron wave vector.
[d] Debye–Waller factor.
[e] Residual factor.
Fourier transform range: 30–130 nm^{-1} for Pt L_{III}-edge and 35–145 nm^{-1} for Mo K-edge; Fourier filtering range: 0.10–0.35 nm^{-1} for Pt L_{III}-edge and 0.10–0.30 nm^{-1} for Mo K-edge.

structures of molybdenum oxides are heterogeneously distributed on the MgO surface, judgement of coordination structure by the EXAFS analysis would be difficult. Nevertheless, an octahedral Mo structure model on the MgO surface in Fig. 9(b) fits the EXAFS data, where an octahedral Mo structure was placed on a lattice oxygen site, which geometrically predicts the Mo–Mg length observed experimentally.

3.2.1.2. Reaction- and reduction-induced structural changes in Pt and Mo sites. The structures of the $[PtMo_6]/MgO$ catalyst after propane dehydrogenation reactions for 4 h at 573 and 723 K and after reduction with hydrogen at 773 K for 2 h were studied by EXAFS. The Fourier transforms and the curve fitting results for the catalysts after the reactions at 573 and 723 K are shown in Fig. 11 and Table 4.

After the C_3H_8 dehydrogenation at 723 K for 2 h the platinum ions were reduced ($Pt^{4+} \rightarrow Pt^0$). The EXAFS oscillation was reproduced by assuming Pt–Pt bond as shown in Fig. 11(a-2). The size of the platinum particles formed in the reaction conditions at 723 K can be estimated using the correlation between the coordination number obtained from the EXAFS analysis and the morphology of the metal particles [22]. Assuming a spherical shape, the Pt particles were estimated as 1.0 ± 0.4 nm in diameter (Fig. 12(b)), which coincides with the dispersion (H/Pt) of 0.7 ± 0.1.

On the contrary, the propane dehydrogenation at 573 K did not induce a similar change. As shown in Fig. 11(b), the Fourier transform was intermediate between them for the Pt ion on the surface and the metallic Pt particle, which implies that the platinum atoms were partially reduced under the conditions at 573 K. The EXAFS oscillation of Fig. 11(b-2) is entirely different from that of Fig. 11(a-2). The coordination number of Pt–Pt bond was determined to be 4.4 (Table 4), the value corresponding to 4 for an octahedral Pt_6 framework. Besides Pt–Pt bonds the contribution of Pt–O and Pt–Mg bondings to the EXAFS oscillation was confirmed by the curve fitting analysis. The distances and coordination numbers of Pt–O and Pt–Mg bonds were determined to be 0.203 nm and 1.1, and 0.303 nm and 2.4, respectively

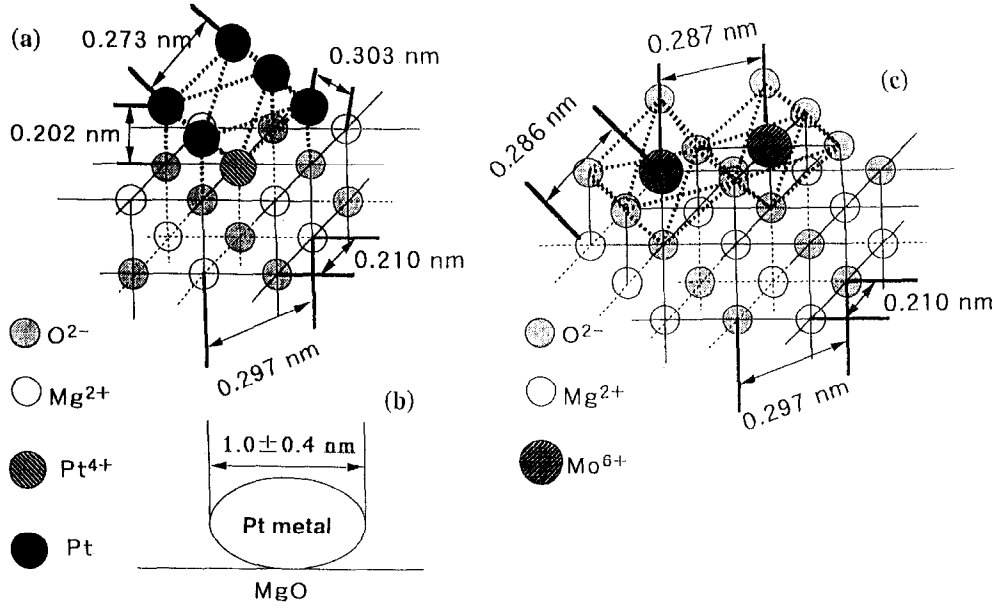

Fig. 12. Model structures around Pt (a, b) and Mo (c) atoms for the $[PtMo_6]/MgO$ catalyst in propane dehydrogenation reactions at 573 K(a) and 723 K (b, c). Part of the oxygen atoms in the octahedral framework in (c) are probably removed under the reaction at 723 K.

(Table 4). If we put five platinum atoms on an unreduced Pt^{4+} ion at the MgO surface to make an octahedral structure with the bond distances of 0.273, 0.202, and 0.303 nm for Pt–Pt, Pt–O and Pt–Mg, respectively, as shown in Fig. 12(a), we can predict the averaged coordination numbers of Pt–O, Pt–Mg and Pt–Pt to be 1.5, 2.0 and 4.0, respectively. These values coincide well with the observed values, 1.1 ± 0.4, 2.4 ± 0.5 and 4.4 ± 0.9, if one takes account of the experimental errors for the coordination numbers determined by EXAFS. Thus it may be concluded that about 80% of Pt ions are reduced and nucleated on the rest of the unreduced Pt ions to make six-nuclear Pt clusters under the propane dehydrogenation conditions at 573 K. A proposed structure is illustrated in Fig. 12(a).

Concerning the local structure of Mo atoms of the $[PtMo_6]/MgO$ catalyst, the molybdenum atoms were not reduced at all at 573 K. The EXAFS data (Table 4) were almost the same as those for the calcined catalyst (Table 2). After the propane dehydrogenation at 723 K, Mo–Mo bond peak newly appeared in the range of 0.2–0.3 nm in the Fourier transform of Fig. 8(b), which is much different from Fig. 8(a) for the catalyst before the reaction. The appearance of Mo–Mo bond at 0.287 nm and the coordination number of 1.5 indicate that at least two distorted octahedral Mo species were connected each other. The bond distance of 0.287 nm is much shorter than 0.331 nm for Mo–Mo bond in the $[PtMo_6O_{24}]^{8-}$ cluster with a Mo^{6+} oxidation state. Spilt over hydrogen atoms from Pt particles can reduce the Mo species at 723 K, by which a part of the oxygen atoms in the octahedral Mo framework may be removed, resulting in reduction of the Mo ions. We tentatively propose a local structure around Mo atoms in Fig. 12(c), which is compatible with the lattice structure of MgO.

3.2.2. *Conventionally prepared monometallic and bimetallic catalysts*

3.2.2.1. Pt–Mo / MgO catalysts. EXAFS spectra of conventionally prepared Pt–Mo/MgO catalysts were compared with those of the ensemble catalyst to check possible structural differences arising from the difference in the preparation method because performance of the

Table 5
Curve fitting results of the Pt L_{III}-edge and Mo K-edge EXAFS spectra obtained from the Pt–Mo/MgO catalyst after calcination at 773 K and after interaction with C_3H_8 at 723 K

	Bond	N [a]	R [b] (nm)	ΔE_0 [c] (eV)	σ [d] (nm)	R factor [e] (%)
Calcination at 773 K	Pt–O	6.3 ± 0.9	0.203 ± 0.001	10.7 ± 3.0	0.0064 ± 0.0010	
	Pt–Mg	9.3 ± 1.3	0.303 ± 0.001	7.3 ± 3.0	0.0084 ± 0.0010	0.4
	Pt–O	5.2 ± 0.9	0.359 ± 0.001	-2.5 ± 3.0	0.0064 ± 0.0010	
	Mo–O	1.8 ± 0.4	0.174 ± 0.001	-4.7 ± 4.0	0.0064 ± 0.0011	1.0
	Mo–Mg	2.2 ± 0.6	0.278 ± 0.001	10.3 ± 4.0	0.0100 ± 0.0011	
After C_3H_8 reaction at 723 K	Pt–O	1.2 ± 0.3	0.203 ± 0.001	8.9 ± 3.0	0.0064 ± 0.0010	
	Pt–Mg	4.1 ± 0.5	0.303 ± 0.001	8.3 ± 3.0	0.0084 ± 0.0010	1.8
	Pt–Pt	4.7 ± 0.9	0.273 ± 0.001	-1.6 ± 3.0	0.0077 ± 0.0010	
	Mo–O	1.6 ± 0.4	0.177 ± 0.001	10.2 ± 4.0	0.0071 ± 0.0012	
	Mo–Mg	4.0 ± 0.7	0.286 ± 0.001	15.6 ± 4.0	0.0060 ± 0.0012	1.9
	Mo–Mo	2.7 ± 0.6	0.288 ± 0.001	-3.3 ± 4.0	0.0087 ± 0.0012	

[a] Coordination number.
[b] Bond distance.
[c] The energy difference between the origins of the photoelectron wave vector.
[d] Debye–Waller factor.
[e] Residual factor.
Fourier transform range: 30–130 nm^{-1} for Pt L_{III}-edge and 35–145 nm^{-1} for Mo K-edge; Fourier filtering range: 0.10–0.35 nm^{-1} for Pt L_{III}-edge and 0.10–0.30 nm^{-1} for Mo K-edge.

Pt–Mo/MgO catalysts in the alkane dehydrogenation reactions was much different from that of the $[PtMo_6]/MgO$ catalyst. The EXAFS analysis results of the Pt–Mo/MgO catalysts after calcination at 773 K and after propane dehydrogenation at 723 K are shown in Table 5. From the EXAFS data and the Mo K-pre-edge peak intensity (Fig. 10) it is suggested that, in this catalyst too, after calcination at 773 K Pt^{4+} ions substituted Mg^{2+} atoms of the MgO support, while Mo^{6+} ions were located on the MgO surface in a distorted octahedral coordination. The coordination number (9.3) of Pt–Mg bond was, however, larger than that (8.1) for the $[PtMo_6]/MgO$ catalyst, suggesting that a part of Pt ions in the Pt–Mo/MgO catalyst was incorporated deeply into the MgO lattice by calcination at 773 K. The clearer differences in the EXAFS data between $[PtMo_6]/MgO$ and Pt–Mo/MgO arose after interaction with propane at 723 K. As shown in Table 5, Pt–O and Pt–Mg bonds besides Pt–Pt bonds were observed in the case of the Pt–Mo/MgO catalyst. Pt ions at the surface should be reduced to the metallic state in the propane dehydrogenation at 723 K. The reason that Pt–O and Pt–Mg bonds are still observed may be due to the location of Pt ions in the MgO lattice. We can estimate the ratio of unreduced Pt ions to the whole Pt atoms in the Pt–Mo/MgO catalyst by using the coordination number of Pt–Pt bond, assuming the formation of Pt particles with a similar size to 1.0 nm for $[PtMo_6]/MgO$. The estimated ratio of unreduced Pt atoms was 0.33. We can also estimate the ratio of unreduced Pt ions by using the coordination number of Pt–Mg bond. The estimated ratio of unreduced Pt ions was 0.35. The obtained values by both estimation are in good agreement. Therefore, it is argued that these unreduced platinum atoms are located at Mg^{2+} sites in the bulk of the MgO support, while the reduced Pt atoms are located on the MgO surface. After propane dehydrogenation on Pt–Mo/MgO at 723 K, Mo–Mo bonds appeared as in the case of $[PtMo_6]/MgO$ (Table 5). The coordination number (2.7) of

Table 6
Curve fitting results of the Pt L_{III}-edge and Mo K-edge EXAFS spectra for the Pt–Mo/MgO (Cl-free) catalyst after calcination at 773 K and C_3H_8 dehydrogenation reactions at 573 and 723 K

	Bond	N [a]	R [b] (nm)	ΔE_0 [c] (eV)	σ [d] (nm)	R factor [e] (%)
Calcination at 773 K	Pt–O	5.9 ± 0.9	0.203 ± 0.001	11.5 ± 3.0	0.0066 ± 0.0010	
	Pt–Mg	6.6 ± 1.2	0.302 ± 0.001	7.9 ± 3.0	0.0086 ± 0.0010	0.7
	Pt–O	4.5 ± 0.9	0.359 ± 0.001	−2.5 ± 3.0	0.0060 ± 0.0010	
	Mo–O	1.5 ± 0.4	0.176 ± 0.001	−4.3 ± 4.0	0.0056 ± 0.0011	2.0
	Mo–Mg	3.9 ± 0.7	0.282 ± 0.001	13.3 ± 4.0	0.0109 ± 0.0011	
After reaction with C_3H_8 at 573 K	Pt–O	1.9 ± 0.5	0.203 ± 0.001	11.1 ± 3.0	0.0064 ± 0.0012	
	Pt–Mg	3.4 ± 0.6	0.303 ± 0.001	9.3 ± 3.0	0.0086 ± 0.0012	2.9
	Pt–Pt	4.1 ± 0.9	0.273 ± 0.001	−0.1 ± 3.0	0.0077 ± 0.0012	
	Mo–O	1.6 ± 0.4	0.175 ± 0.001	−0.3 ± 4.0	0.0060 ± 0.0012	
	Mo–Mg	2.8 ± 0.7	0.280 ± 0.001	15.0 ± 4.0	0.0093 ± 0.0012	2.0
After reaction with C_3H_8 at 723 K	Pt–Pt	6.9 ± 1.3	0.271 ± 0.001	−4.5 ± 3.0	0.0093 ± 0.0012	4.0
	Mo–O	1.7 ± 0.4	0.177 ± 0.001	10.0 ± 4.0	0.0066	
	Mo–Mg	3.7 ± 0.7	0.286 ± 0.001	15.7 ± 4.0	0.0055	1.7
	Mo–Mo	2.0 ± 0.4	0.288 ± 0.001	−4.4 ± 4.0	0.0082	

[a] Coordination number.
[b] Bond distance.
[c] The energy difference between the origins of the photoelectron wave vector.
[d] Debye–Waller factor.
[e] Residual factor.
Fourier transform range: 30–130 nm^{-1} for Pt L_{III}-edge and 35–145 nm^{-1} for Mo K-edge. Fourier filtering range: 0.10–0.35 nm^{-1} for Pt L_{III}-edge and 0.10–0.30 nm^{-1} for Mo K-edge.

Mo–Mo bond was about twice that (1.5) for the $[PtMo_6]/MgO$ catalyst. This may be referred to clusterization/aggregation of molybdates in the Pt–Mo/MgO catalyst.

The curve fitting results obtained from EXAFS analysis of the Pt–Mo/MgO (Cl-free) catalysts are shown in Table 6. After calcination at 773 K, the similar structures around Pt and Mo atoms to those for $[PtMo_6]/MgO$ were observed, with difference in the coordination number of Pt–Mg bond. The coordination number of 6.6 for Pt–Mg bond is far deviated from the value predicted if all Pt ions substitute Mg^{2+} ions at the surface top layer of MgO. Some of the Pt atoms were reduced during the propane dehydrogenation reaction at 573 K, but the coordination number of Pt–Mg bond (3.4) may also hold the similar structural picture to that for $[PtMo_6]/MgO$. Thus the local structure of Pt sites in the Pt–Mo/MgO (Cl-free) catalyst seems to be less homogeneous compared with the $[PtMo_6]/MgO$ ensemble catalyst. The difference between the Cl-free and residual Cl-containing catalysts may be attributed to electronic interactions between the platinum and chlorine atoms that possibly favors incorporation of platinum atoms into MgO bulk.

3.2.2.2. Monometallic Pt / MgO and Mo / MgO catalysts. To obtain details of the structure around the Pt and Mo atoms from more simple samples, monometallic Pt/MgO, Mo/MgO and Pt/MgO (Cl-free) catalysts were also examined by EXAFS. The curve fitting results are summarized in Table 7. The coordination numbers of Pt–Mg bonds in the Pt/MgO catalyst and the Pt/MgO (Cl-free) catalyst calcined at 773 K were 9.8 and 6.2, respectively, which are similar to 9.3 and 6.6 for the Pt–Mo/MgO catalyst and the Pt–Mo/MgO (Cl-free) catalyst, respectively, but larger or smaller than 8.1 for the $[PtMo_6]/MgO$ catalyst. Local structures around Pt atoms of Pt–Mo/MgO and Pt/MgO were not distinguishable from each other, nor were those of Pt–Mo/MgO (Cl-free) and Pt/MgO (Cl-free). Again, local structures around Mo atoms among the $[PtMo_6]/MgO$, Pt–Mo/MgO (Cl-free), and Mo/MgO catalysts were not distinguishable.

3.2.3. Catalytically active sites

EXAFS analysis of the fresh catalysts (Tables 2, 4–7) shows the difference in the coordination number of the Pt–Mg bonds. In Fig. 13, there is a decreasing trend in isobutane yield

Table 7
Curve fitting results of the Pt L_{III}-edge and Mo K-edge EXAFS spectra for the Pt/MgO, Mo/MgO and Pt/MgO (Cl-free) catalysts after calcination at 773 K

	Bond	N [a]	R [b] (nm)	ΔE_0 [c] (eV)	σ [d] (nm)	R factor [e] (%)
Pt/MgO	Pt–O	6.3 ± 0.9	0.203 ± 0.001	11.1 ± 3.0	0.0064 ± 0.0010	
	Pt–Mg	9.8 ± 1.2	0.303 ± 0.001	7.3 ± 3.0	0.0084 ± 0.0010	0.3
	Pt–O	5.4 ± 0.8	0.361 ± 0.001	−0.2 ± 3.0	0.0064 ± 0.0010	
Mo/MgO	Mo–O	1.8 ± 0.4	0.176 ± 0.001	−2.4 ± 4.0	0.0060 ± 0.0011	
	Mo–Mg	3.5 ± 0.8	0.284 ± 0.001	15.7 ± 4.0	0.0098 ± 0.0010	1.0
Pt/MgO (Cl-free)	Pt–O	5.9 ± 0.9	0.202 ± 0.001	11.1 ± 3.0	0.0069 ± 0.0010	
	Pt–Mg	6.2 ± 1.1	0.301 ± 0.001	7.9 ± 3.0	0.0090 ± 0.0010	0.2
	Pt–O	6.1 ± 0.8	0.360 ± 0.001	−1.6 ± 3.0	0.0074 ± 0.0010	

[a] Coordination number.
[b] Bond distance.
[c] The energy difference between the origins of the photoelectron wave vector.
[d] Debye–Waller factor.
[e] Residual factor.
Fourier transform range: 30–130 nm^{-1} for Pt L_{III}-edge and 35–145 nm^{-1} for Mo K-edge; Fourier filtering range: 0.10–0.35 nm^{-1} for Pt L_{III}-edge and 0.10–0.30 nm^{-1} for Mo K-edge.

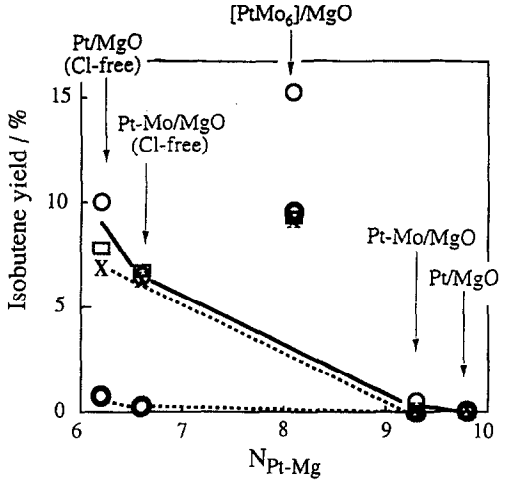

Fig. 13. Yield of isobutene at 723 (□, ×) and 773 K (○, ○) as a function of the coordination number of Pt–Mg bonds in the examined catalysts; □, ○ after 10 min reaction, ×, ○: after 180 min reaction.

observed for the conventionally prepared Pt-containing catalysts upon increasing coordination number of Pt–Mg bonds, which indicates that the activity reduces significantly as bonding of Pt atoms with the support increases. Clarke et al. [23] showed that with Pt/MgO catalysts in hydrogenolysis reactions of C_5 and C_6 hydrocarbons that there is a shift of negative charge from the magnesia O^{2-} ions to platinum atoms. It is noteworthy that the interaction between Pt and MgO was found to increase by the presence of residual chlorine in the catalyst. The authors left open an explanation of which of the different catalytic properties in their experiments owe their origin to possible morphological changes in the metal clusters induced by chlorine. In the present study it is clear that Cl-containing catalysts are far less active than the corresponding Cl-free ones. Combined EXAFS and catalytic results shown in Fig. 13 may elucidate the role of chlorine since it is evident that it leads to stronger interactions of platinum with the support through the increased number of Pt–Mg bonds. The increase of the Pt–Mg coordination number in the Cl-containing samples indicates that Pt atoms probably locate in deeper surface layers of MgO. The decreasing trend of the activity observed in Fig. 13 for the conventionally prepared catalysts may then be attributed to the incorporation of Pt atoms to deeper sites in the MgO bulk. Comparison of the catalytic properties of the catalysts studied is rather complicated since many parameters influencing the catalytic performance should be taken into account.

The Pt and Mo atoms in the conventionally prepared catalysts may be randomly distributed at the surface, whereas the special preparation method using the $[PtMo_6O_{24}]^{8-}$ precursor is expected to induce some additional parameters that could influence its catalytic performance. In fact, $[PtMo_6]/MgO$ does not follow the decreasing trend observed for the rest of the catalysts as expected from the coordination number of its Pt–Mg bonds (Fig. 13). The presence of the molybdates surrounding the Pt atoms in a special way probably influences positively catalytic activity of platinum. Furthermore, according to the EXAFS analysis, it is most likely that all of the platinum atoms of the ensemble catalyst locate on the first surface layer of MgO, optimizing the catalytic performance of the ensemble catalyst.

Leclercq et al. [24] studied the kinetics of hydrogenolysis of butane over $Pt–Mo/SiO_2$ catalysts with various Mo/(Mo + Pt) ratios and distinguished hydrogenolysis of the two different kinds of C–C bonds. It was shown that the addition of Mo to Pt drastically changes the selectivity of the reaction but this selectivity is approximately the same for all the bimetallic Pt–Mo catalysts, it does not vary with the metal composition. The adsorption equilibrium constants were found to be the same for all Pt–Mo catalysts, which shows that on all Pt–Mo catalysts butane adsorbs on the same mixed Pt–Mo site with a constant composition whatever the catalyst composition. They argued that the active sites are mixed sites composed of Pt and Mo atoms [24]. The method for preparation of $[PtMo_6]/MgO$ in the present study led to the creation of catalysts with an organized surface

geometry with advanced catalytic performance in alkane dehydrogenation reactions. Calcination of the impregnated catalyst under oxygen at 773 K results in substitution of Mg^{2+} atoms of the support with Pt^{4+} atoms. The platinum ions located in the top layer of the support surface are reduced under the reaction conditions to form small clusters anchored on their own ions at 573 K. The clusters are converted to highly dispersed Pt particles under the high temperature reaction conditions (at 723 K). The observed high activity of the ensemble catalyst originates mainly from the large number of 'working sites'.

The active structure of $[PtMo_6]/MgO$ produced in situ under the reaction conditions at 573 K is not destroyed during the reactions at temperatures up to 723 K, as revealed by our experiments. On the contrary, this structure was destroyed by treatment with hydrogen at 773 K and the catalytic properties became similar to those of the conventionally prepared catalysts. Reduction with hydrogen at 773 K does not seem to influence significantly the size of the Pt particles, judging from the coordination number of Pt–Pt bond (Table 4). Instead, the high temperature reduction seems to modify the local structure of the Mo atoms and hence the ensemble structure of Pt and Mo. As shown in Table 2, Tables 4 and 5, there is an increasing trend in the coordination number of Mo–Mo bond as activity of the catalysts at 723 K decreases: $[PtMo_6]/MgO$ (1.5) > Cl-free Pt–Mo/MgO (2.0) > Pt–Mo/MgO (2.7). Reduction of the $[PtMo_6]/MgO$ catalyst with H_2 at 773 K caused a significant increase of N_{Mo-Mo} ($1.5 \rightarrow 2.5$) and N_{Mo-Mg} ($3.5 \rightarrow 6$) which resulted in a dramatic drop in activity and stability (Fig. 8(b)). The large increase in N_{Mo-Mo} and N_{Mo-Mg} may reflect the decrease in the Mo oxidation state and the incorporation of reduced Mo atoms into the surface layers of MgO. In contrast no change occurred on the catalytic performance of the conventionally prepared Cl-free Pt–Mo/MgO catalyst after the same treatment, indicating that the surface of this catalyst had already become the undesirable one during the catalytic reaction.

The special arrangement of molybdates around platinum particles in the $[PtMo_6]/MgO$ catalyst stabilizes the active sites and enables the sites to remain uncovered by inactive species either by inhibiting by-processes that produce coke or by removing carbonaceous residue from the active surface to the support. The low selectivity of the ensemble catalyst towards C_1–C_3 (C_1–C_2 for propane) hydrocarbon byproducts may indicate a rather weak chemisorption of the reacting alkane. Further investigation may be needed for more information about the active sites of the catalyst composed of Pt and Mo sites.

4. Conclusions

(1) The framework of the $[PtMo_6O_{24}]^{8-}$ precursor was broken upon impregnation on MgO. Calcination of the fresh sample at temperatures above 673 K under oxygen atmosphere induced interactions between the precursor and the MgO support, giving rise to the appearance of Pt–Mg and Mo–Mg bonds.

(2) The proposed structures of Pt and Mo atoms after calcination of the sample at 773 K for 2 h are shown in Fig. 9. According to this model, platinum atoms in the 4+ state are located at the first surface layer of MgO (100) substituting Mg^{2+} ions of the support. Molybdenum atoms in the 6+ state are located on the MgO surface in a distorted, octahedral coordination, while there is no observable interaction between Pt and Mo atoms.

(3) The EXAFS analysis for $[PtMo_6]/MgO$ presents direct evidence on the replacement of metal ions of the first layer of support surface by supported metal ions during calcination above 673 K.

(4) During propane dehydrogenation at 573 K small Pt clusters grew on the unreduced Pt^{4+} atoms (Fig. 12(a)), while no observable change occurred with the local structure of Mo atoms,

which maintained the Mo structure of the calcined catalyst.

(5) Treatment at the higher reaction temperature (723 K) or reduction with hydrogen at 773 K led to complete reduction of the platinum atoms to form small metallic particles on the MgO surface with an average diameter of 1.0 nm (Fig. 12(b)). Under the same conditions the partially reduced molybdates in the $[PtMo_6]$/MgO catalyst linked with each other on the MgO surface, showing a dimer structure on average.

(6) In the Pt–Mo/MgO catalyst, two thirds of the platinum ions were located on the first surface layer of MgO, while the rest one third were located at Mg^{2+} sites in the MgO bulk. The Pt ions in the bulk were not reduced even at 773 K-reduction conditions.

(7) The difference in structure between Pt–Mo/MgO and Pt–Mo/MgO (Cl-free) may be attributed to an electronic interaction between Pt and Cl atoms which possibly favors incorporation of Pt atoms into MgO bulk.

(8) The performance of the $[PtMo_6]$/MgO ensemble catalyst for butane, isobutane and propane dehydrogenation reactions was found to be more active, selective and resistant to deactivation due to coke formation, than the Pt–Mo/MgO, Pt–Mo/MgO (Cl-free), Pt/MgO, Pt/MgO (Cl-free), Pt/Al_2O_3, and Mo/MgO catalysts.

(9) The residual Cl-containing catalysts were far less active and deactivated more rapidly than the corresponding Cl-free ones.

(10) The decreasing trend of the activity for the conventionally prepared catalysts was observed as a function of increasing coordination number of Pt–Mg bond, which is attributed to the incorporation of Pt atoms to deeper layers of the MgO bulk.

(11) However, the activity of the $[PtMo_6]$/MgO catalyst did not follow this trend and was much higher than that predicted from this decreasing line. This is attributed to some additional parameters generated from the preparation method by use of the inorganic cluster $[PtMo_6O_{24}]^{8-}$ with a plane ensemble structure.

References

[1] G.C. Bond, Catalysis by Metals, Academic Press, London, 1962.
[2] Y. Zhu, R.G. Minet and T.T. Tsotsis, Catal. Lett., 18 (1993) 49.
[3] T. Ioannides and G.R. Gavalas, J. Membr. Sci., 77 (1993) 207.
[4] Z.X. Chen, A. Derking, W. Koot and M.P. van Dijk, to be published.
[5] V. Ponec and G.C. Bond, Catalysis by Metal Alloys, Elsevier, Amsterdam, 1995.
[6] U. Lee and Y. Sasaki, Chem. Lett., (1984) 1297.
[7] T. Liu, Y. Matsui, U. Lee, K. Asakura and Y. Iwasawa, Catalytic Science and Technology, Vol. 1, Kodansha, Tokyo, 1991, p. 267.
[8] T. Liu, K. Asakura, U. Lee, Y. Matsui and Y. Iwasawa, J. Catal., 135 (1992) 367.
[9] EXAFS analysis program EXAFSH, coded by T. Yokoyama and T. Ohta, The University of Tokyo (1993).
[10] J.J. Rehr and R.C. Albers, Phys. Rev., B41 (1990) 8139.
[11] J.J. Rehr, J. Mustre de Leon, S.I. Zabinsky and R.C. Albers, J. Am. Chem. Soc., 113 (1991) 5135.
[12] J. Mustre de Leon, J.J. Rehr, S.I. Zabinsky and R.C. Albers, Phys. Rev., B44 (1991) 4146.
[13] F.W. Lytle, P.S.P. Wei, R.B. Greegor, G.H. Via and J.H. Sinfelt, J. Chem. Phys., 70 (1979) 4849.
[14] J.A. Horsley, J. Chem. Phys., 76 (1982) 1451.
[15] D.R. Short, A.W. Mansour, J.W. Cook, Jr., D.E. Sayers and J.R. Katzer, J.Catal., 82 (1983) 299.
[16] A.N. Mansour, J.W. Cook and D.E. Sayers, J. Phys. Chem., 88 (1984) 2330.
[17] H. Onishi, C. Egawa, T. Aruga and Y. Iwasawa, Surf. Sci., 191 (1987) 479.
[18] C.T.J. Mensch, J.A.R. van Veen, B. van Wingerden and M.P. van Dijk, J. Phys. Chem., 92 (1988) 4961.
[19] S.R. Bare, G.E. Mitchell, J.J. Maj, G.E. Vrieland and J.L. Gland, J. Phys. Chem., 97 (1993) 6048.
[20] S.-C. Chang, M.A. Leugers and S.R. Bare, J. Phys. Chem., 96 (1992) 10358.
[21] E. Shimao, Bull. Chem. Soc. Jpn., 40 (1967) 1609.
[22] R.B. Greegor and F.W. Lytle, J. Catal., 63 (1980) 476.
[23] J.K.A. Clarke, M.J. Bradley, L.A. Garvie, A.J. Craven and T. Baird, J. Catal., 143 (1993) 122.
[24] G. Leclercq, A. El Gharbi and S. Pietrzyk, J. Catal., 144 (1993) 118.